NSRRC-J04375 (2014)

Nanoscale

PAPER

View Article Online
View Journal | View Issue

Published on 13 November 2013. Downloaded by National Tsing Hua University on 07/07/2014 02:09:42.

Cite this: *Nanoscale*, 2014, 6, 2194

Solution self-assembly and phase transformations of form II crystals in nanoconfined poly(3-hexyl thiophene) based rod-coil block copolymers†

Yi-Huan Lee,[ab] Yi-Lung Yang,[b] Wei-Che Yen,[b] Wei-Fang Su[bc] and Chi-An Dai*[ab]

Solution processing of π-conjugated polymers constitutes a major low-cost manufacturing method for the fabrication of many new organic optoelectronic devices. The solution self-assembly kinetics of π-conjugated rod-coil block copolymers of symmetric poly(3-hexyl thiophene)-*b*-poly(2-vinyl pyridine) (P3HT-P2VP) during drying and the phase transformations of the subsequently dried samples were studied by using a combination of TEM, SAXS, WAXS and DSC measurements. During solution drying in chlorobenzene, a good solvent for the copolymer, P3HT-P2VP first formed nanoseed aggregates followed by the directional growth of nanofibrils driven by the formation of prevailing form II P3HT crystals within its nanofibril core confined by the surrounding domain of P2VP blocks. This result was in sharp contrast when a similar molecular weight P3HT homopolymer was solution self-assembled in chlorobenzene, nearly free from confinement, in which case the resulting nanofibrils consisted of a mixture of majority form I and form II crystals. Solvent-cast films of P3HT-P2VP nanofibrils with form II crystals were heat-/cold-treated and showed solid-state phase transformations from form II crystals to form I crystals, both within nanofibrils with annealing, indicating the metastability of the form II crystals with temperature. A disordered state followed with increasing temperatures which, when cooled, induced the formation of a thermodynamically stable lamellar phase with only form I P3HT crystals. Correspondingly, the study provides new strategies for controlling polymorphs and nanostructures of π-conjugated block copolymers for future applications using solution processing and subsequent heat treatment.

Received 9th August 2013
Accepted 10th November 2013

DOI: 10.1039/c3nr04214f

www.rsc.org/nanoscale

Introduction

During the past decades, regioregular poly(3-hexylthiophene) (rr-P3HT) has attracted much attention for uses in low-cost, large-area, and flexible optoelectronic devices such as light emitting diodes, thin film transistors and solar cells due to its unique optoelectronic properties.[1–6] It has been widely accepted that the electrical properties of these fabricated devices are critically dependent on the crystalline structure of the P3HT films, which is often caused by the solution-processing conditions and post-treatment methods.[7–12] Two types of crystalline structures of P3HT have been identified, *i.e.*, forms I and II.[12–15] The main difference between these two crystalline polymorphs is the shorter *a*-axis lattice spacing for the form II crystals that resulted from the interdigitation of their side-chains compared with that of the form I crystals with minimum overlapping. It should be noted that most of previous studies were mainly focused on form I crystals which were often obtained from solution casting or thermal treatment processes for high molecular weight P3HT.[14,16] Specific efforts to fabricate pristine P3HT form II crystals have been demonstrated, however, are less common.[15] Therefore, clarifying the crystal formation of P3HT during the film preparation process continues to be a research topic of utmost importance.

Recently, there has been a growing interest in synthesizing P3HT based block copolymers since it may offer a new strategy for the organization of the π-conjugated polymers and synergistically improve their mechanical and optoelectronic properties for device applications.[17–25] The morphology, optoelectronic property, and application in devices for these P3HT based block copolymers were investigated actively. Despite continuous improvement in device performance, solution-phase self-assembly of these conjugated block polymers, especially in their polymorphic-microstructure development, has not yet been well understood. In order to fully exploit these materials for future applications, a detailed study on the morphology evolution of

[a]*Department of Chemical Engineering, National Taiwan University, No. 1, Roosevelt Rd. Sec. 4, Taipei 106, Taiwan. E-mail: polymer@ntu.edu.tw; Fax: +886-2-2362-3040; Tel: +886-2-3366-3051*

[b]*Institute of Polymer Science and Engineering, National Taiwan University, Taipei 106, Taiwan*

[c]*Department of Materials Science and Engineering, National Taiwan University, Taipei 106, Taiwan*

† Electronic supplementary information (ESI) available: Detailed synthesis procedures and characterization data (NMR, GPC and XRD) of polymer samples. See DOI: 10.1039/c3nr04214f

This journal is © The Royal Society of Chemistry 2014

Published on 13 November 2013. Downloaded by National Tsing Hua University on 07/07/2014 02:09:42.

P3HT based block copolymers prepared with various processing parameters (solvents, drying conditions, thermal annealing, *etc.*) is greatly required.

In this study, we investigated the structure evolution of a symmetric rod-coil P3HT-P2VP block copolymer sample prepared *via* a slow solution drying approach and subsequent heat treatment of the dried samples. The choice of a symmetric sample was considered mainly because of its potential to self-organize into continuous nanochannels or interpenetrated networks for which P3HT may facilitate easy charge transport for advanced utilization. Surprisingly, a fiber morphology, wherein the P3HT molecular chains were arranged in form II crystals was obtained. Notably, the self-assembly behavior of P3HT-P2VP was found to be significantly different from that of a parent P3HT homopolymer, which showed mixtures of form I and form II crystals. To the best of our knowledge, this is the first case showing the formation of predominately P3HT form II crystals in a P3HT based block copolymer system. We propose that this phenomenon can be attributed mainly to the consequence of the slow crystallization of the P3HT block under the influence of the nanoconfinement effect from the neighboring P2VP blocks on the crystal growth during the drying process. Furthermore, the temperature-dependent phase transformations of the solvent-dried P3HT-P2VP thin film including the order–disorder, order–order transitions of the rod-coil P3HT-P2VP block copolymers and the crystalline polymorphic transition of P3HT segments were also revealed. We believe that these observations allow a detailed understanding of the dependence of self-assembly of P3HT based block copolymers on both kinetic and thermodynamic effects and offer guidance for the control of hierarchical structures and optoelectronic properties in solution processing and thermal treatment of π-conjugated block copolymer systems.

Experimental section

Synthesis of PPP-P3HT block copolymers

A symmetric P3HT-P2VP$_{48}$ diblock copolymer (M_n = 9600 g mol^{-1}, M_w/M_n = 1.17, volume fraction of P3HT = 0.48), hereafter referred to as TP48, used in this study was synthesized by the anionic macroinitiation method in THF described previously.[20] For comparison, a P3HT homopolymer with a similar molecular weight to that of the P3HT block in TP48 was also synthesized. The detailed characterizations of these polymers are described in the ESI.† All molecular parameters for the synthesized polymer samples used for the current study are tabulated in Table 1.

Table 1 Summary of the characteristics of P3HT-P2VP samples

Sample[a]	M_n of P3HT (g mol^{-1})	M_n of P2VP (g mol^{-1})	PDI	%HT[b]	f	ϕ[d]
P3HT	4500	—	1.20	>92%	100%	100%
TP48	4500	5100	1.17	>92%	46%	48%

[a] TP48: designation of P3HT-P2VP block copolymers. [b] Estimated by using ^{1}H NMR from the P3HT homopolymer precursor. [c] Weight fraction of P3HT in copolymers as measured by ^{1}H NMR. [d] Volume fraction of P3HT in copolymers calculated by utilizing density values 1.10 g cm^{-3} for P3HT and 1.14 g cm^{-3} for P2VP.

Solvent-cast samples prepared from slow solution drying

Polymer films were prepared by dissolving the polymers in chlorobenzene to make a 1 wt% solution, followed by slow drying of the solution in a controlled environment of constant temperature (25 °C) and humidity environment (40% RH). Chlorobenzene (CB) was chosen as the solvent for depositing the film samples since it's a common solvent for P3HT and widely used for fabricating optoelectronic devices with high performance.[5,26] The solution was placed on a microbalance in order to record its solvent weight loss to track its structure evolution during different drying times. The as-prepared dried sample had film thickness of 0.1 mm after 2 months of drying.

Transmission electron microscopy (TEM)

TEM samples for the investigation of solution-phase self-assembly of polymer solutions were prepared by depositing a droplet of polymer solution onto a carbon-coated copper grid, followed by drying the sample by exposure to air for 3 hours. Additionally, TEM samples for the structural characterization of polymer films were prepared by embedding pieces of solvent-dried TP48 samples in resin, followed by curing the sample at 60 °C for 24 h. Subsequently, thin slices of polymer samples having a thickness of about 70 nm were obtained by a Reichert Ultracut microtome at room temperature. The cut samples were stained by exposing them to the vapor of iodine for 12 hours. Bright field images and selected-area electron diffraction (SAED) were performed on a JEOL 1230EX operating at 100 kV with a Gaten Dual Vision CCD Camera.

Small-angle and wide-angle X-ray scattering (SAXS and WAXS)

SAXS and WAXS experiments were performed separately at the 23A1 and 13A1 endstations at the National Synchrotron Radiation Research Center (NSRRC) in Taiwan. The wavelengths of the incident beam were 1.18095 Å for the SAXS and 1.03051 Å for the WAXS measurements, respectively. For the SAXS measurements, the scattering patterns were collected on a Mar-CCD with a diameter of 165 mm. The one-dimensional scattering profiles were obtained by integration of the two-dimensional pattern and reported as plots of the scattering intensity, I, *versus* the scattering vector, q. The scattering vector q was calibrated using a standard sample of Ag-behenate. For the WAXS measurements, the one-dimensional scattering patterns were collected using a point detector and reported as plots of the scattering intensity *versus* the scattering vector, with the value of q calibrated using standard samples of Ag-behenate and Si powder. For the temperature scan of the X-ray scattering spectra, the polymer samples were heated in-line with a PID controlled heating unit to the specified temperature under a dried nitrogen environment for 10 min before the X-ray spectra are collected.

Published on 13 November 2013. Downloaded by National Tsing Hua University on 07/07/2014 02:09:42.

Differential scanning calorimetry (DSC)

DSC measurements were performed using a Perkin-Elmer Diamond® differential scanning calorimeter equipped with an intracooler. All polymer samples, typically ~5 mg, were sealed in aluminum pans for the DSC analysis. The measurements were carried out by heating/cooling the samples between 0 °C and 220 °C at a heating/cooling rate of 10 °C min^{-1}. The temperature and heat flow scales at the measured heating rate was carefully calibrated using standard materials.

Results and discussion

To study the crystallization behavior of the solvent-cast fully dried P3HT-P2VP sample, static WAXS measurements on the TP48 sample were first carried out and the result was compared with that of the parent P3HT homopolymer. As shown in Fig. 1(a), the scattering pattern of the solvent-cast P3HT homopolymer sample has at least 10 reflections corresponding to the crystallographic planes associated with typical P3HT form I and form II crystalline structures, while the WAXS spectrum of the solvent-cast TP48 sample shows diffraction reflections associated mainly with form II crystalline structures. The low-angle $(100)_I$ and $(100)_{II}$ reflections indicate the 16.6 and 11.9 Å interlayer distances separated by the alkyl side chain of P3HT for the form I and form II structures, respectively, and the diffraction peaks located at 15.3° and 13.5° correspond to the $(020)_I$ and $(020)_{II}$ reflections, which is the distance between the stacking of the main chain layers for the form I and the form II structures, respectively.[12–14] The detailed structures of the unit cell for the form I and form II crystallites are schematically depicted in Fig. 1(c) and (d), respectively. Notably, the main difference between these two crystalline polymorphs is the shorter *a*-axis repeat distance of the form II crystals as compared with that of form I crystals resulting from interdigitation of their side chains. For the solvent-cast dried P3HT sample, its WAXS data are consistent with the results of previous reported studies that mixtures of form I and from II crystals are usually obtained by the solution deposition method for low molecular weight P3HT homopolymers (<7000 g mol^{-1}).[12,14] However, the discovery of a mainly form II crystalline structure in the block copolymer sample was surprising since overlapping between hexyl side chains within neighboring main chain stacks is unstable and should therefore be minimal.[13] Remarkably, the P2VP block might impart a profound geometric effect on crystallization behavior of the P3HT block during the solution-phase self-assembly, which resulted in the unusual crystalline phase of mainly form II crystals. Therefore, to understand the origin of this phenomenon, solution-phase structural evolution of the TP48 sample in CB were conducted under different solution drying times during the slow drying process.

Fig. 2(a) shows the solution concentration of the TP48 sample plotted against the drying time, which could be adopted to reflect the solution self-assembly kinetics. Additionally, the corresponding color changes of the copolymer solution were also recorded, as shown in Fig. 2(b). In polar organic solvents such as chlorobenzene (CB) where both polymer blocks are soluble, P3HT-P2VP in CB exhibits light orange color, revealing that the block exists as an isolated chain. After 3 days of drying, the light orange solution had turned dark, and TEM analysis (Fig. 3(a)) showed the formation of small micelles with a core size of 10 nm. As the TP48–CB solution was further dried from 3 days to 25 days, the color of the solution changed from dark orange to light brown and then to dark brown. This color change could be attributed to the crystallization-driven self-assembly of P3HT-P2VP copolymers from seed micelles to nanorods and then to nanofibrils during the drying period,[27,28] and the corresponding morphology evolution could be confirmed in the TEM images, as shown in Fig. 3(b)–(d). Note that the SAED pattern of the TP48 sample shown in the inset picture of Fig. 3(d) shows an apparent form II crystalline structure (020) diffraction ring. This observation implied that the P3HT block organized into a form II structure rather than a form I structure during the solution-phase self-assembly. To the best of our knowledge, this is the first case showing the formation of P3HT form II crystals in the P3HT based block

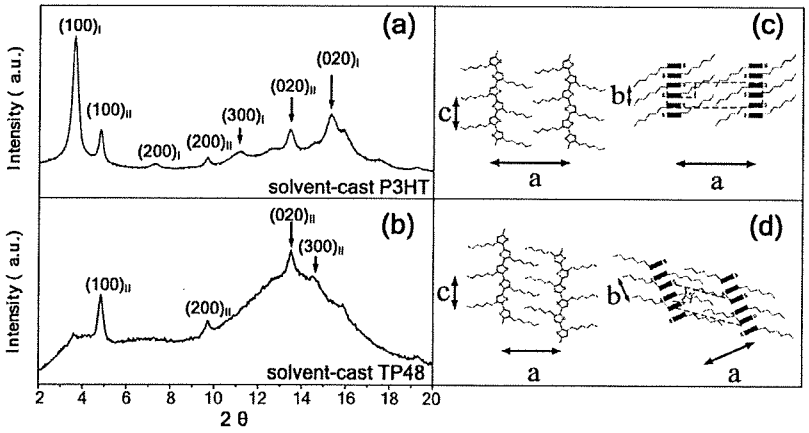

Fig. 1 The WAXS spectra of solvent-cast (a) P3HT homopolymer and (b) TP48 block copolymer. A mixture of the form I and form II crystals was observed for the solvent-cast P3HT homopolymer, while predominantly form II crystals were formed for the solvent-cast TP48 block copolymer. A schematic drawing is plotted for (c) the form I and (d) form II crystalline structures of P3HT.

This journal is © The Royal Society of Chemistry 2014

Published on 13 November 2013. Downloaded by National Tsing Hua University on 07/07/2014 02:09:42.

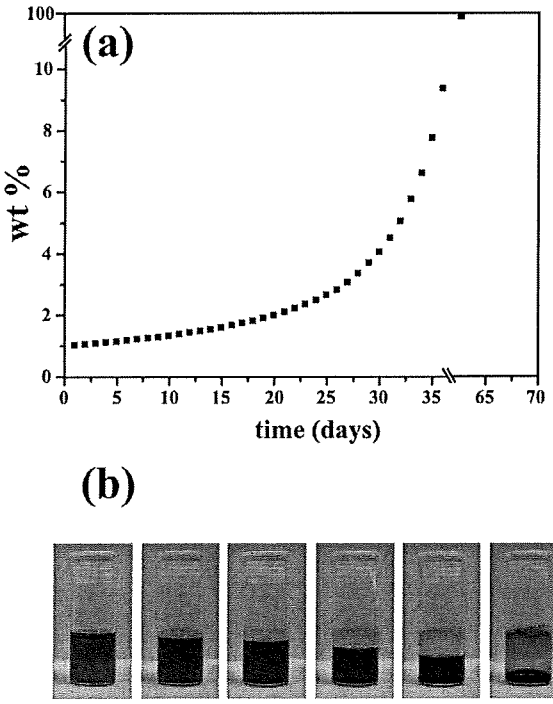

Fig. 2 (a) Concentration of the TP48–CB solution plotted against the drying time. (b) Color changes of the TP48–CB solution dried after different times of 0, 3, 8, 15, 25, and ~60 days (from left to right).

copolymer system during the solution self-assembly process. We speculate that this result can be attributed to the consequence of the crystallization of the P3HT block under the influence of the nanoconfinement effect of the surrounding P2VP block. During the slow drying process, there is enough time for the P3HT chains to overcome the crystallization energy barrier and stack into the form II crystalline structure in the liquid phase. Simultaneously, the surrounding P2VP blocks further impart a confinement effect by serving as an outer corona layer around the P3HT crystalline cores, thereby restricting the space for the crystallization of P3HT blocks, resulting in the P3HT crystals that favor the structure with overlap of the side chains to minimize the interlayer distance of crystals. Therefore, in contrast to the crystallization behavior of the P3HT homopolymers, which was mainly free from any confining domains, the packing of the P3HT blocks in the TP48 sample showed high fractions of the form II crystalline structure.

Upon drying for 60 days, the polymer samples were completely dried, resulting in a 0.1 mm-thick film with dark brown color, as shown in the right picture of Fig. 2(a). In order to understand the microstructure of this copolymer in the solid state, the morphology of the TP48 film were investigated by using TEM. Fig. 4(a) shows the TEM image for an as-cast TP48 sample, in which the dark region in the micrograph corresponds to the P2VP domain stained with iodine while the white region corresponds to the P3HT domain without any iodine staining. From the TEM micrograph, the formation of a nanowire structure with its fibril long-axis orienting randomly and extending in length for several hundred nanometers can be observed. SAED measurement was also performed to illustrate the P3HT crystallographic structure within the nanofibrillar morphology (shown in the inset picture of Fig. 4(a)), which

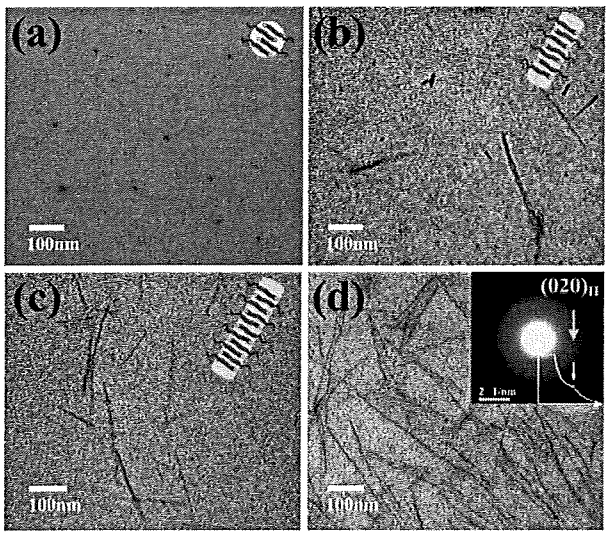

Fig. 3 TEM micrographs of TP48–CB solution at different drying times. (a) 3 day: nanoseed micelles, (b) 8 days: nanoseeds and nanorods, (c) 15 days: nanorods and (d) 25 days: nanofibrils. The inset picture in (d) shows the corresponding SAED pattern of TP48 nanofibrils with a form II (020) crystalline plane. In addition, the SAED patterns are azimuthally integrated and plotted in the inverse space to show the exact peak position (indicated by the arrow) for the form II crystals.

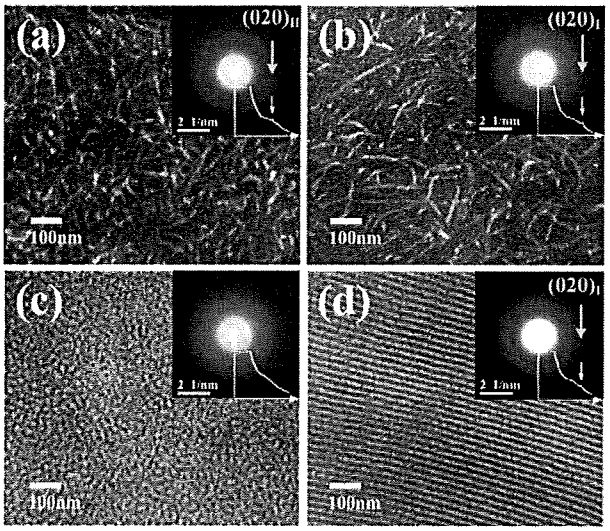

Fig. 4 TEM micrographs of the solvent-cast TP48 film annealed at different temperatures. (a) A fibril-like structure of the as-cast TP48 sample, (b) a view of the solvent-cast TP48 sample annealed at 120 °C, (c) a disordered structure observed for TP48 annealed above 180 °C and (d) a lamellar structure of TP48 annealed above 180 °C followed by annealing at 100 °C for 24 h. The inset pictures in (a)–(d) show the corresponding SAED patterns of TP48 annealed at their respective temperatures. In addition, the SAED patterns are azimuthally integrated and plotted in the inverse space to show different peak positions (indicated by the arrow) for form I and form II crystals.

Published on 13 November 2013. Downloaded by National Tsing Hua University on 07/07/2014 02:09:42.

shows the formation of P3HT form II crystals and is consistent with the static WAXS spectrum of the solvent-cast fully dried TP48 sample. On the basis of these experimental results, it can be concluded that the P3HT segments in the interpenetrated nanofibrillar P3HT-P2VP domain exhibited a crystalline packing of the form II structure. For full-dried TP48 annealed at 120 °C, its TEM image (Fig. 4(b)) also exhibits a fiber-like morphology similar to that of the as-cast sample. The morphological result demonstrates that the nanowire phase is preserved from the as-cast room temperature to 120 °C. The SAED pattern of the 120 °C sample (the inset picture in Fig. 4(b)) shows an obvious form I $(020)_I$ diffraction ring as indicated by the solid arrows. Compared to that of the as-cast TP48 sample, the stacking distance of the main chains in the 120 °C sample decreased slightly from 4.4 to 3.8 Å, indicating a structural reorganization of the P3HT segments from form II crystals into the form I structure without changing the overall fibril nanostructure. As TP48 was further heated above 180 °C, an obvious change in the TEM images revealed a morphological transformation from fibril structures to a disordered phase (shown in Fig. 4(c)). At the same time, the SAED pattern of the disordered region showed no visible diffraction rings (as shown in the inset picture of Fig. 4(c)), indicating that the P3HT blocks existed as random coils at 180 °C. Upon cooling the sample from 180 °C to 100 °C, the TP48 sample self-assembled into a lamellar nanostructure with form I crystals, as shown in Fig. 4(d) and in the inset SAED figure.

To further identify the polymorphism and phase transformation of the solvent-cast fully dried TP48 sample during the heating process, step-wise in-line heating SAXS/WAXS and differential scanning calorimetry (DSC) measurements were also performed. Fig. 5(a) shows the temperature evolution of 1D SAXS profiles for the TP48 sample heated from 40 °C to 180 °C. The corresponding SAXS spectrum for the TP48 sample annealed at 40 °C revealed a very shallow and barely visible primary scattering peak that corresponds to a nanofibrillar structure at this temperature. As the temperature increases to 140 °C, the intensity of the primary peak of TP48 suddenly decays. This sudden decrease indicates that there is a fibril structure to disordered phase transformation for the TP48 sample annealed at 140 °C. Above 160 °C, the residual primary peak is still visible due to the local density fluctuation of the two components of the block copolymer in the disordered phase and the peak position shifts toward the lower wavevector with further increasing temperature, indicating that the disordered domain expands with increase in the temperature. Additionally, Fig. 5(b) shows a representative WAXS pattern of the annealed TP48 sample as a function of temperature. As the sample's temperature increases from 40 °C to 100 °C, the intensity of the diffraction peaks related to the form II structure gradually decays while those corresponding to the form I type crystal become distinctly visible. These scattering features demonstrate that the TP48 sample undergoes a direct solid-state transformation of crystalline modification through side chain melting, which serves to modify the location of main-chain stacking.[29] It should also be noted that the temperature at which the polymorphic transition of form II to form I for the TP48

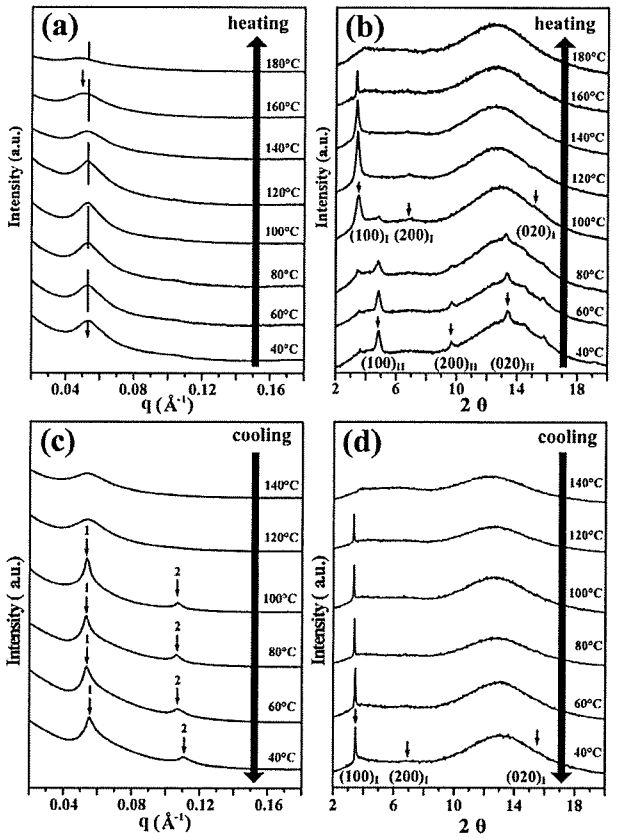

Fig. 5 The step-wise heating (a) SAXS and (b) WAXS spectra for the solvent-cast TP48 sample. After the samples were melted, step-wise cooling (c) SAXS and (d) WAXS spectra were collected.

sample occurs is significantly higher than that of the P3HT homopolymer (shown in Fig. S6†). Such an increase may be due to the nanoconfinement effects resulting from the restriction of the neighboring microphase separated P2VP domains on the block copolymer. Above 80 °C, the $(100)_I$ diffraction peak for TP48 becomes significantly larger than that of form II crystals, indicating crystallization of the form I crystals aided by a drastic increase in P2VP chain mobility as the TP48 sample is heated above its glass transition temperature. Upon further heating the sample to ~120 °C, new sharp and intense diffraction patterns associated with $(100)_I$ and $(020)_I$ planes emerge, showing the formation of the form I crystal structure at the expense of from II crystals. At a temperature of 160 °C, the WAXS pattern of TP48 corresponds to the diffraction only from a weak (100) plane, indicating a nematic liquid crystalline structure of P3HT.[30,31] For temperatures above 180 °C, TP48 exhibits no visible diffraction peaks, indicating that the P3HT is amorphous above its melting temperature. In summary, the temperature dependent WAXS patterns of solvent-cast TP48 show that there is a series of phase transitions from the originally well-packed form II crystals, to form I crystals, to nematic liquid crystals, and finally to an isotropic phase with increasing temperature. Note that the phase transitions observed from the in-line heating WAXS experiments compared favorably with the results of the

This journal is © The Royal Society of Chemistry 2014

Published on 13 November 2013. Downloaded by National Tsing Hua University on 07/07/2014 02:09:42.

DSC measurements (see Fig. 6), in which we observed several endothermic peaks centered near 100 °C, 120 °C, and 170 °C corresponding to the melting of P3HT forms II crystals, melting of ordered form I packing, melting of the nematic phase, and finally a nematic-to-isotropic phase transition, respectively. However, it is difficult to assign the melting of hexyl side chains at about 60 °C in the DSC curve due to a possible signal mergence with that of the glass transition temperature ($T_{g\ P2VP}$) of the P2VP block. Fig. 5(c) and (d) further shows the structural transformation observed in step-wise cooling SAXS/WAXS experiments. As TP48 was cooled from the melt in the isotropic state, we first observe nematic ordering at 120 °C. As the sample was further cooled to 40 °C from the nematic phase, the copolymer sample self-assembled into the lamellar structure with P3HT form I crystals. Upon further heating/cooling cycles, it can be observed that the transition from the lamellar structure with form I crystals to the isotropic phase *via* the nematic phase is thermally reversible. Consistently, in the DSC cooling run, we observed the isotropic-to-nematic transition at ~130 °C, the crystallization exothermic transition of P3HT form I crystals at 110 °C and the glass transition of P2VP at 50 °C.[32]

Based on the combined results of TEM, SAED, SAXS/WAXS, and DSC measurements on the TP48 sample during the slow drying procedure, followed by the step-wise heating/cooling treatment, we observed that there was a complicated polymorphism and phase transformation in the solvent-cast P3HT-P2VP block copolymer. A schematic illustration detailed showing the structure evolution in the solution phase and phase transformation including the order–disorder, order–order and polymorphism transitions in the solid phase of the TP48 sample is shown in Fig. 7. Upon slow solution drying, the morphology evolution is a result of the intricate balance between the packing forces and the intermolecular interactions between the constituting blocks. Therefore, the P3HT-P2VP block copolymers are a useful platform to study nanoconfinement effects from the connecting P2VP coil block on the solution behavior of 1-dimensional P3HT polymer rod-like crystals. For the solid-phase self-assembly of the TP48 films, several important features should be noted as follows: (1) the form II to form I crystallographic transition occurred in the nanowire nanodomains. (2) The temperature range of morphological transforms from a nanowire phase to a disorder phase is higher than $T_{g\ P2VP}$ and consistent with that of crystal to amorphous transition. These experimental results gave an indication that the nanofibrillar structure formed from solution drying significantly dominated the following phase behavior upon heating and the chain mobility of the P2VP block associated with the morphological changes was relatively subtle. Upon cooling the sample from the melt, the presence of the lamellar structure rather than the occurrence of the nanowire phase indicated that the self-assembly behavior of the copolymers was mainly driven by the microphase segregation strength. The formation of the ordered lamellar phase reflected the need for the symmetric TP48 sample to minimize the interfacial energy and the amount of stretching that both P2VP as well as the conjugated P3HT blocks must sustain in order for space-filling and to maintain a uniform segmental density. Simultaneously, the increasing rod–rod interaction of the P3HT block due to the undercooling of the polymers improves the anisotropic ordering of P3HT chains, resulting in the P3HT form I crystals in the lamellar structural environment. As a consequence, our experimental

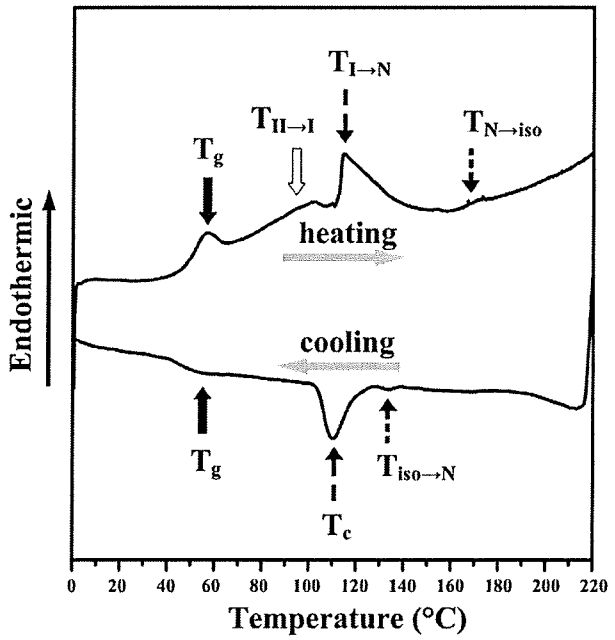

Fig. 6 DSC traces of solvent-cast TP48 of the first heating run and subsequent cooling run from its melt state. In the heating run, the solid arrow indicates the glass transition temperature of the P2VP block, the hollow arrow shows the endothermic transition of P3HT form II crystals into form I crystals, the dashed arrow indicates the transition of form I crystals into a nematic phase, and the dotted arrows indicate the endothermic enthalpy peak associated with the nematic-to-isotropic phase transformation, respectively. In the cooling run, the dashed arrow indicates the exothermic crystallization transition of P3HT form I crystals.

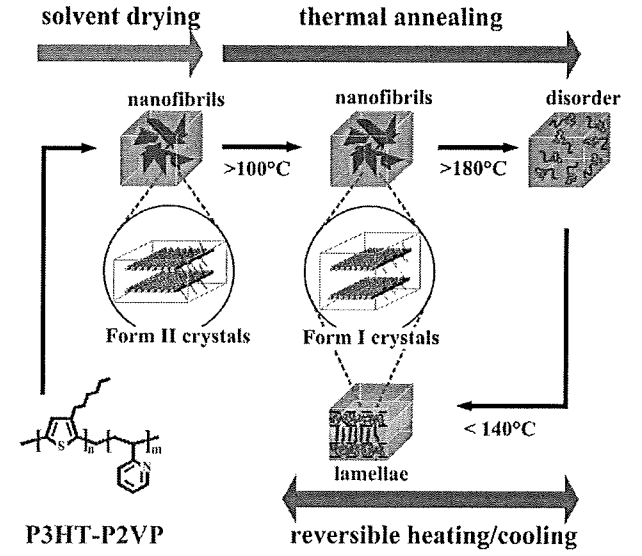

Fig. 7 Schematic representations of the phase transformations for solution dried TP48 block copolymers.

Published on 13 November 2013. Downloaded by National Tsing Hua University on 07/07/2014 02:09:42.

results demonstrate that the polymorph and the nanostructure of P3HT based block copolymers can be tailored by different approaches such as solution drying or heating/cooling treatments and provide new insights into the rod-coil block copolymer system for further applications.

Conclusion

In this study, the solution phase self-assembly of symmetric rod-coil P3HT-P2VP block copolymers was first investigated through a slow solution drying process. Based on the structural results, it was found that the copolymer–CB solution displays a nanowire structure with predominately P3HT form II crystals, indicating a consequence of the slow crystallization of the P3HT block under the influence of the nanoconfinement effect from the neighboring P2VP block on the crystalline P3HT core during solution drying. As the polymer sample was completely dried, TEM, SAXS, WAXS, and DSC were subsequently used to explore the detailed phase transformation of the P3HT-P2VP solvent-dried film. These measurements demonstrated that the TP48 sample undergo a form II to form I crystallographic transition in the nanowire nanodomains followed by the phase transformation to a nematic state and then to an isotropic phase upon heating. Upon cooling from the disordered melt, it can be observed that the morphology changed from the isotropic phase to the nematic phase and then to the lamellar structure with form I crystals, and these phase transformations are thermally reversible. As a consequence, our results shows promise for the practical usage of self-assembling rod-coil block copolymers containing P3HT since the resulting self-assembly of P3HT-P2VP block copolymers offers a level of structural control that is important for future applications.

Acknowledgements

The financial support from the National Science Council of Taiwan is greatly appreciated. The X-ray measurements were conducted at the National Synchrotron Radiation Research Center (NSRRC) in Taiwan. The authors would also like to thank Dr U-Ser Jeng and Dr Ming-Tao Lee for their help during the X-ray experiments at NSRRC.

References

1 G. M. Wang, J. Swensen, D. Moses and A. J. Heeger, *J. Appl. Phys.*, 2003, **93**, 6137–6141.
2 F. Padinger, R. S. Rittberger and N. S. Sariciftci, *Adv. Funct. Mater.*, 2003, **13**, 85–88.
3 J. Liu, T. Tanaka, K. Sivula, A. P. Alivisatos and J. M. J. Frechet, *J. Am. Chem. Soc.*, 2004, **126**, 6550–6551.
4 G. Li, V. Shrotriya, J. Huang, Y. Yao, T. Moriarty, K. Emery and Y. Yang, *Nat. Mater.*, 2005, **4**, 864–868.
5 W. L. Ma, C. Y. Yang, X. Gong, K. Lee and A. J. Heeger, *Adv. Funct. Mater.*, 2005, **15**, 1617–1622.
6 H. Sirringhaus, *Adv. Mater.*, 2005, **17**, 2411–2425.
7 H. Yang, S. W. LeFevre, C. Y. Ryu and Z. N. Bao, *Appl. Phys. Lett.*, 2007, **90**, 172116.
8 L. H. Nguyen, H. Hoppe, T. Erb, S. Günes, G. Gobsch and N. S. Sariciftci, *Adv. Funct. Mater.*, 2007, **17**, 1071–1078.
9 G. Li, Y. Yao, H. Yang, V. Shrotriya, G. Yang and Y. Yang, *Adv. Funct. Mater.*, 2007, **17**, 1636–1644.
10 C. W. Chu, H. Yang, W. J. Hou, J. Huang, G. Li and Y. Yang, *Appl. Phys. Lett.*, 2008, **92**, 103306.
11 Y. D. Park, H. S. Lee, Y. J. Choi, D. Kwak, J. H. Cho, S. Lee and K. Cho, *Adv. Funct. Mater.*, 2009, **19**, 1200–1206.
12 S. Joshi, S. Grigorian, U. Pietsch, P. Pingel, A. Zen, D. Neher and U. Scherf, *Macromolecules*, 2008, **41**, 6800–6808.
13 T. J. Prosa, M. J. Winokur, J. Moulton, P. Smith and A. J. Heeger, *Macromolecules*, 1992, **25**, 4364–4372.
14 A. Zen, M. Saphiannikova, D. Neher, J. Grenzer, S. Grigorian, U. Pietsch, U. Asawapirom, S. Janietz, U. Scherf, I. Lieberwirth and G. Wegner, *Macromolecules*, 2006, **39**, 2162–2171.
15 J. Liu, Y. Sun, X. Gao, R. Xing, L. Zheng, S. Wu, Y. Geng and Y. Han, *Langmuir*, 2011, **27**, 4212–4219.
16 S. Joshi, P. Pingel, S. Grigorian, T. Panzner, U. Pietsch, D. Neher, M. Forster and U. Scherf, *Macromolecules*, 2009, **42**, 4651–4660.
17 J. S. Liu, E. Sheina, T. Kowalewski and R. D. McCullough, *Angew. Chem., Int. Ed.*, 2002, **41**, 329–332.
18 K. Sivula, Z. T. Ball, N. Watanabe and J. M. J. Fréchet, *Adv. Mater.*, 2006, **18**, 2–6.
19 C. Müller, S. Goffri, D. W. Breiby, J. W. Andreasen, H. D. Chanzy, R. A. J. Janssen, M. M. Nielsen, C. P. Radano, H. Sirringhaus, P. Smith and N. Stingelin-Stutzmann, *Adv. Funct. Mater.*, 2007, **17**, 2674–2679.
20 C.-A. Dai, W.-C. Yen, Y.-H. Lee, C.-C. Ho and W.-F. Su, *J. Am. Chem. Soc.*, 2007, **129**, 11036–11038.
21 B. W. Boudouris, C. D. Frisbie and M. A. Hillmyer, *Macromolecules*, 2008, **41**, 67–75.
22 I. Botiz and S. B. Darling, *Macromolecules*, 2009, **42**, 8211–8217.
23 S. J. Park, S. G. Kang, M. Fryd, J. G. Saven and S. J. Park, *J. Am. Chem. Soc.*, 2010, **132**, 9931–9933.
24 Y.-H. Lee, W.-C. Yen, W.-F. Su and C.-A. Dai, *Soft Matter*, 2011, **7**, 10429–10442.
25 S.-H. Lin, S.-J. Wu, C.-C. Ho and W.-F. Su, *Macromolecules*, 2013, **46**, 2725–2732.
26 G. Li, V. Shrotriya, Y. Yao, J. Huang and Y. Yang, *J. Mater. Chem.*, 2007, **17**, 3126–3140.
27 S. K. Patra, R. Ahmed, G. R. Whittell, D. J. Lunn, E. L. Dunphy, M. A. Winnik and I. Manners, *J. Am. Chem. Soc.*, 2011, **133**, 8842–8845.
28 J. B. Gilroy, D. J. Lunn, S. K. Patra, G. R. Whittell, M. A. Winnik and I. Manners, *Macromolecules*, 2012, **45**, 5806–5815.
29 Y. Yuan, J. Zhang and J. Sun, *Macromolecules*, 2011, **44**, 6128–6135.
30 K. Yazawa, Y. Inoue, T. Yamamoto and N. Asakawa, *Phys. Rev. B: Condens. Matter Mater. Phys.*, 2006, **74**, 094204.
31 J. Martín, A. Nogales and M. Martín-González, *Macromolecules*, 2013, **46**, 1477–1483.
32 Z. Wu, A. Petzold, T. Henze, T. Thurn-Albrecht, R. H. Lohwasser, M. Sommer and M. Thelakkat, *Macromolecules*, 2010, **43**, 4646–4653.

This journal is © The Royal Society of Chemistry 2014